crystals

MDPI

Article

Enhanced Electromagnetic Wave Absorption Properties of FeCo-C Alloy by Exploiting Metamaterial Structure

Tang Xuan Duong [1,2,3,†], Do Khanh Tung [1,2,†], Bui Xuan Khuyen [1,2], Nguyen Thi Ngoc Anh [2], Bui Son Tung [1,2,†], Vu Dinh Lam [1], Liangyao Chen [4], Haiyu Zheng [5,6] and YoungPak Lee [4,5,6,*]

1 Graduate University of Science and Technology, Vietnam Academy of Science and Technology, 18 Hoang Quoc Viet, Hanoi 100000, Vietnam; binhnhiduong@gmail.com (T.X.D.); tungdk@ims.vast.ac.vn (D.K.T.); khuyenbx@ims.vast.ac.vn (B.X.K.); tungbs@ims.vast.ac.vn (B.S.T.); lamvd@gust-edu.vast.ac.vn (V.D.L.)
2 Institute of Materials Science, Vietnam Academy of Science and Technology, 18 Hoang Quoc Viet, Hanoi 100000, Vietnam; anhntn@ims.vast.ac.vn
3 Joint Russia-Vietnam Tropical Science and Technology Research Center, 63 Nguyen Van Huyen, Hanoi 100000, Vietnam
4 Optical Science and Engineering, Fudan University, Shanghai 200433, China; lychen@fudan.ac.cn
5 Department of Physics, Quantum Photonic Science Research Center and RINS, Hanyang University, Seoul 04763, Republic of Korea; haiyu@hanyang.ac.kr
6 Alpha ADT Co., Ltd., Hwaseong 18469, Republic of Korea
* Correspondence: yplee@hanyang.ac.kr
† These authors contributed equally to this work as co-correspondence.

Abstract: This study presents a tri-layer broadband metamaterial absorber that operates in the GHz range. The absorber was composed of a polyhedral iron-cobalt alloy/graphite nanosheet material arranged in a flat sheet with two punched-in rings for the top layer, a continuous FR-4 layer at the middle, and a continuous copper layer at the bottom. For the normal incidence of the electromagnetic wave, the proposed absorber demonstrated an exceptional broadband absorption in a frequency range of 7.9–14.6 GHz, revealing an absorption exceeding 90%. The absorption magnitude remains to be above 90% in a frequency range of 8–11.1 GHz for transverse-electric-polarized waves at incident angles up to 55°. For both the transverse-magnetic- and electric-polarized waves, the absorption exceeds 90% in a frequency range of 9.5–14.6 GHz. The physical mechanism behind the absorption properties is analyzed thoroughly through the electric and magnetic field distributions. The obtained results could contribute potentially to the development of microwave applications based on metamaterial absorbers, such as radar-stealth technology, electromagnetic shielding for health safety, and reduced electromagnetic interferences for high-performance communications and electronic devices.

Keywords: metamaterials; broad-band absorption; iron-cobalt alloy; electromagnetic coupling

Citation: Duong, T.X.; Tung, D.K.; Khuyen, B.X.; Anh, N.T.N.; Tung, B.S.; Lam, V.D.; Chen, L.; Zheng, H.; Lee, Y. Enhanced Electromagnetic Wave Absorption Properties of FeCo-C Alloy by Exploiting Metamaterial Structure. *Crystals* **2023**, *13*, 1006. https://doi.org/10.3390/cryst13071006

Academic Editor: George Kenanakis

Received: 31 May 2023
Revised: 21 June 2023
Accepted: 21 June 2023
Published: 25 June 2023

1. Introduction

Microwave metamaterial absorbers (MAs) have become an emerging class of materials that have shown great potential in applications such as electromagnetic (EM) wave absorption, stealth technology, and energy harvesting [1]. The absorption of microwave radiation is primarily governed by the interaction between the incident EM waves and the sub-wavelength unit cells of metamaterial structure. This interaction includes the resonance and impedance matching. The resonant absorption occurs when the dimensions of metamaterial unit cells are engineered to match the wavelength of the incident EM waves. This results in a strong interaction between the waves and the resonant structure, leading to the absorption of incident energy. The resonance can be induced by different mechanisms, such as the magnetic and electric resonance, depending on the properties of the metamaterial.

The traditional approaches for the MAs typically rely on the generation of fundamental magnetic or electric resonances through the utilization of circular- or dipole-like currents on the metallic structures. On the other hand, an alternative approach involves integrating the intrinsic magnetic and electric materials directly into the MA structures to generate the desired magnetic or electric responses. In the case of magnetic resonance, the metamaterial unit cells are designed to exhibit a strong response to the magnetic component of incident waves. This is achieved by incorporating magnetic materials, such as FeCo alloys with a high saturation magnetization. The incident waves induce oscillations in the magnetic materials, generating the eddy currents that dissipate energy as heat. This dissipation leads to the absorption of the incident waves and can be effective particularly at microwave frequencies. On the other hand, the electric resonance relies on the interaction between the incident waves and the electric response of the metamaterial structure. This phenomenon is observed commonly in structures incorporating materials with high electrical conductivity, such as nano-carbon materials. The nano-carbon-material-based metamaterials exhibit an exceptional electrical conductivity, enabling the generation of surface plasmons when exposed to the incident waves. These surface plasmons induce resonant absorption, efficiently trapping and absorbing the incident energy. The tunable properties of nano-carbon materials, such as the carrier density and Fermi level, allow us to control the absorption characteristics and to broaden the absorption bandwidth.

Furthermore, impedance matching is a fundamental mechanism in the design of absorbers. Essentially, any absorber structure should be engineered meticulously to align its impedance with that of the surrounding medium. The achievement of impedance matching conditions makes the efficient coupling between incident waves and absorber, leading to a reduction in the reflection and scattering effects. Consequently, the absorber exhibits the maximum absorption of the incoming EM energy [2,3]. For the MAs, the absorption mechanism depends on the specific design and constituent materials of the metamaterial structure [4]. A significant challenge in the microwave MA is the extension of the absorption bandwidth, particularly toward higher frequencies. Researchers have developed several strategies to overcome this challenge [5–7]. One approach includes the design of MA structures with multiple resonant modes, which might expand the absorption spectrum. Another way is to use multilayer structures with varying materials and thicknesses, leading to a gradient of the effective permittivity and permeability, which results in a broad absorption bandwidth.

Recent research has focused on the employment of FeCo and nano-carbon materials for microwave absorption applications. The FeCo-based materials have shown high magnetic permeability and can be magnetized easily, making them well-suited for microwave absorbers based on the magnetic loss [8–10]. Conversely, nano-carbon materials, such as carbon nanotubes or graphene, have high electrical conductivity and can be used for the absorbers in terms of resistive loss [11–15]. Therefore, the incorporation of FeCo nanoparticles into the carbon-based materials has been shown to improve the magnetic loss significantly, while the kind of materials can enhance the electrical conductivity [16–19]. Overall, the use of alloys might lead to the development of more efficient and effective microwave absorbers.

In our work, by exploiting both usual MA and alloy, a novel FeCo/carbon-based metamaterial structure is presented to enhance the microwave absorption. The simulated results demonstrate a remarkable improvement in the absorption bandwidth of proposed MA, compared with that of FeCoC plate backed by the bare copper. We clarify the absorption mechanism by investigating the electric and magnetic field distribution and study the contribution of losses in the MA. Moreover, the effects of polarization and the incident angle on the absorption are examined to evaluate the operational performance of proposed MA.

2. Structural Design and Methods

Figure 1 shows the schematic of the proposed MA, featuring the optimized design for the unit cell. The structure comprises three layers: FeCo/graphite nanosheets (FeCo-C) whose shape looks like a flat sheet with two punched-in rings at the top, a middle

layer of Flame Retardant 4 (FR-4), and a continuous copper plate at the bottom. In our simulation, we used a relative permittivity of FR-4 of 4.3, with a loss tangent of 0.025, and employed the copper layer with a conductivity of 5.8×10^7 S/m. We utilized the polyhedral FeCo/graphite nanosheet material, whose frequency-dependent complex permittivity and permeability were determined experimentally by Xiaogang Su et al. [20], as indicated in Figure 2.

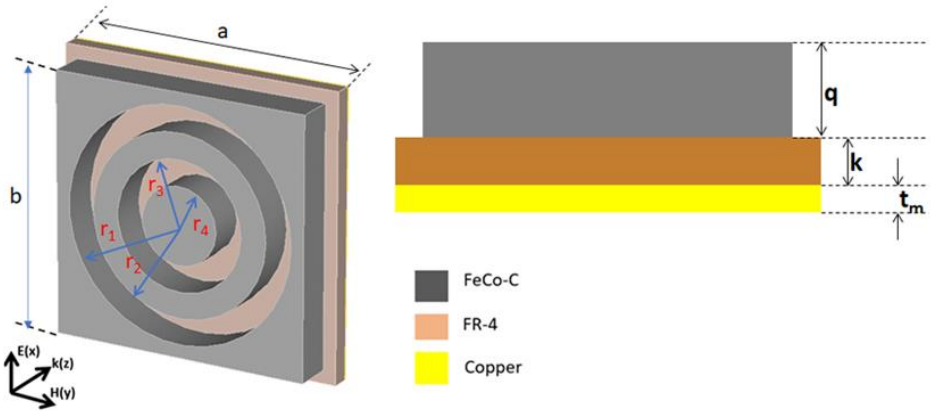

Figure 1. Schematic of the proposed unit cell with the optimized geometrical parameters. a = 22, b = 20, r_1 = 9, r_2 = 7, r_3 = 5, r_4 = 3, q = 3, k = 0.5, t_m = 0.036 mm.

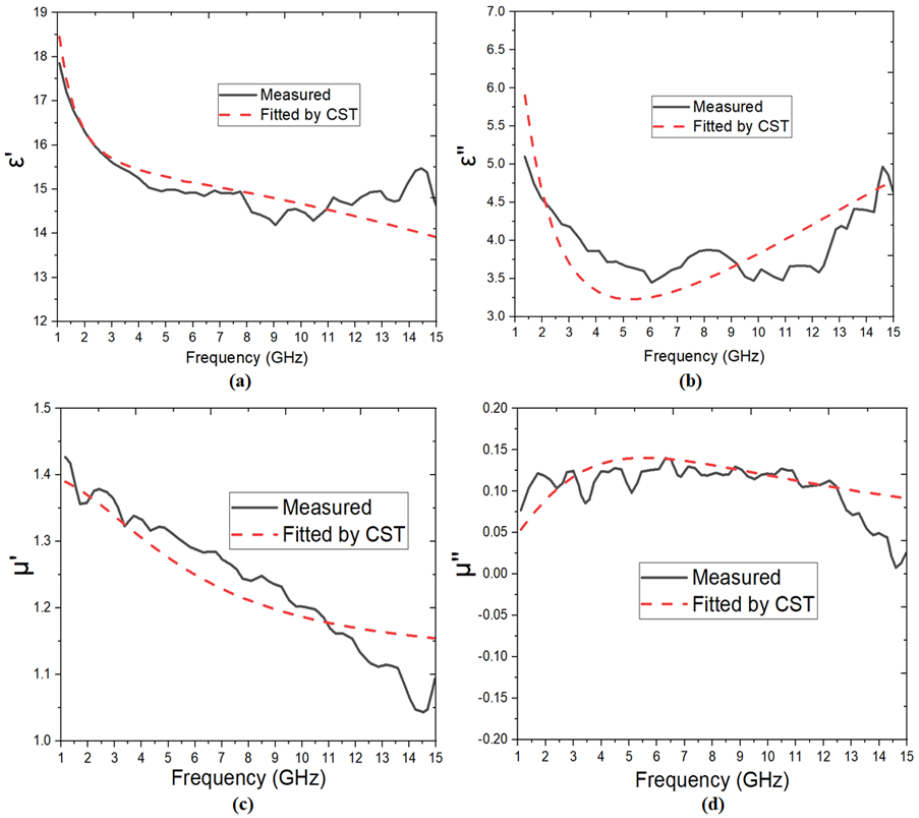

Figure 2. Frequency-dependence of the complex permittivity and permeability of FeCo-C. (**a**) Real ε' and (**b**) imaginary ε'' parts of the permittivity. (**c**) Real μ' and (**d**) imaginary μ'' parts of the permeability. The corresponding measured data are employed from [20] for the fitting.

We used the CST Microwave Studio software [21] to conduct the simulation, employing the frequency domain solver in a frequency range from 1 to 15 GHz. To impose the periodic boundary conditions, we utilized the x- and y-direction. The absorption was calculated by using formula $A(\omega) = 1 - R(\omega) - T(\omega)$, where $R(\omega) = |S_{11}(\omega)|^2$ and $T(\omega) = |S_{21}(\omega)|^2$

were the reflection and transmission, respectively. In our design, the bottom layer was composed of a continuous copper plate, resulting in zero transmission in the microwave region, and thus the absorption simply becomes $A(\omega) = 1 - R(\omega)$.

3. Results and Discussion

In this section, the obtained results have been rigorously investigated through numerical analysis by using the experimental data. The experimental data utilized for the simulations were previously reported in [20].

In order to achieve the optimized structure depicted in Figure 1, the optimizations were conducted on various structural geometries. The objective was to develop a structure with the smallest overall thickness, while ensuring a broad range of absorption with an absorption rate exceeding 90%. The optimization of the MA structure in this study involved the evolution of four types of FeCo-C structures: (1) the previously reported continuous FeCo-C layer, (2) a square-array configuration, (3) a square-array configuration with a punched-in ring, and (4) a square-array configuration with two punched-in rings.

As the initial step, we examined the reflection-loss properties of FeCo-C material, which was utilized on a copper plate [Figure 3a]. The thickness of the FeCo-C layer was changed gradually from 1.6 to 5.3 mm in Figure 3b,c. That of the copper plate was t_m = 0.036 mm. Figure 3b,c display the simulated reflection loss and absorption spectrum, respectively, of FeCo-C according to the layer thickness, which was backed by the copper plate. Our simulated results are in accordance with the reported results in [20], which show only one absorption peak for the continuous FeCo-C layer.

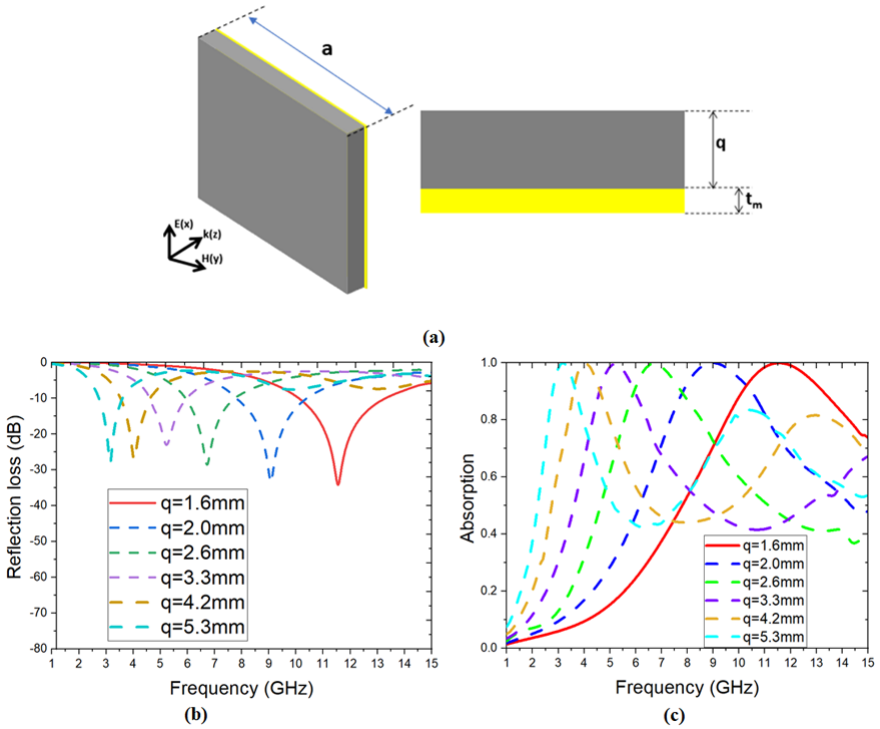

Figure 3. (**a**) Schematic of the FeCo-C structure backed by the copper plate. (**b**) Reflection-loss curve and (**c**) the corresponding absorption spectrum for different layer thicknesses.

Secondly, a simple schematic of the MA was proposed, consisting of three layers: a continuous copper plate at the bottom, a middle layer of FR-4, and a top layer made of a square-array configuration composed of FeCo-C [Figure 4a]. In this modified design, the MA exhibited two absorption peaks at 6.1 and 8.2 GHz, with an absorption above 90% [Figure 4b].

To broaden the absorption bandwidth while ensuring the absorption rate exceeding 90%, further modifications were made to the design of the top layer by incorporating a

punched-in ring structure [Figure 5a]. This adjustment resulted in an extended absorption spectrum, with an absorption continuously above 90% in a frequency range from 7.0 to 9.5 GHz [Figure 5b].

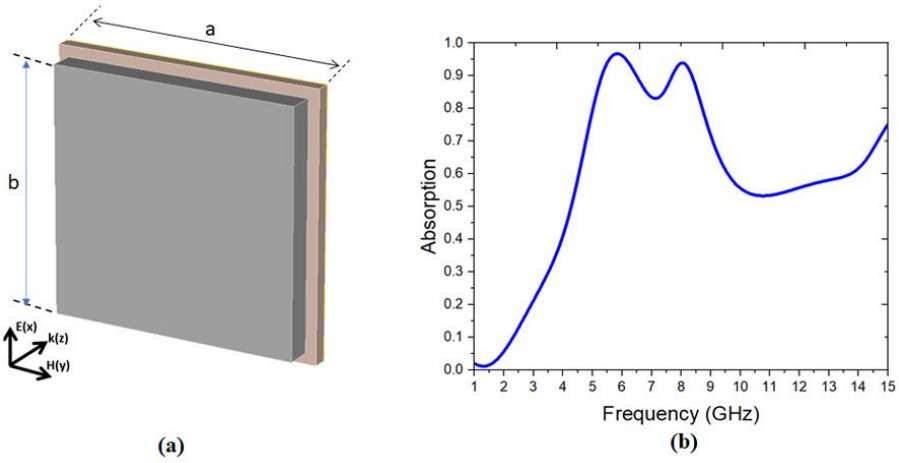

Figure 4. (**a**) Schematic of the MA using a square-array configuration of FeCo-C at the top and (**b**) the absorption spectrum.

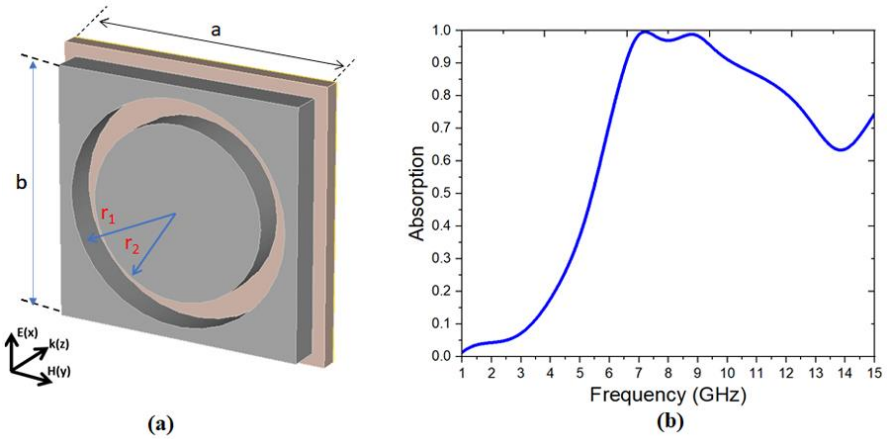

Figure 5. (**a**) Schematic of the MA using a square-array configuration of FeCo-C with a punched-in ring at the top and (**b**) the absorption spectrum.

In the final stage of the structural optimization, an additional punched-in ring was introduced to investigate its impact on the absorption behavior. However, it is important to note that the inclusion of two punched-in rings was limited due to the fixed unit-cell size in our study. Figure 6a shows the absorption spectrum of the optimized MA, based on FeCo-C. The proposed structure exhibits a broadband absorption, with an absorption over 90% in a frequency range of from 7.9 to 14.6 GHz, featuring two peaks with the near-unity absorption at 9.4 and 12.5 GHz, respectively. The absorption spectrum of the FeCo-C-based MA was found to be significantly broader than that of the copper-backed FeCo-C, indicating an improvement in the absorption upon integrating the FeCo-C material into the metamaterial structure. To clarify the role of different layers in the metamaterial structure, the fractions of energy dissipated in the FeCo-C and FR-4 layer are presented in Figure 6b. It is shown that more than 98% of the energy loss occurred in the FeCo-C layer, while the loss in the FR-4 one was limited to only 2%. The energy dissipation results prove that the FeCo-C layer in the MA is the main factor contributing to the broadband absorption.

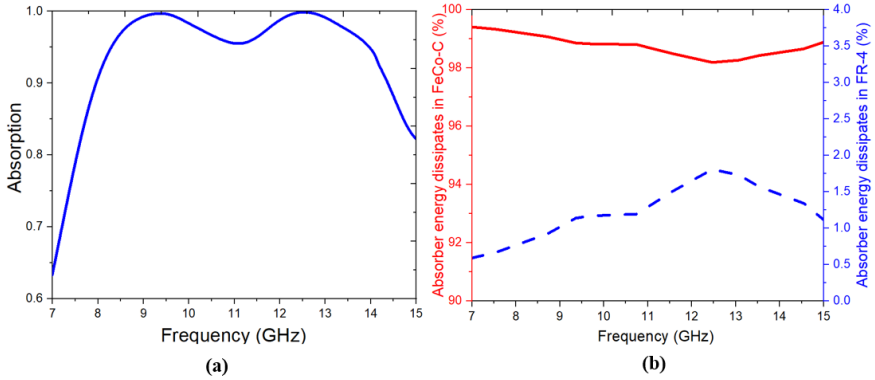

Figure 6. (**a**) Absorption spectrum of the designed MA structure and (**b**) the captured energy dissipated in the FeCo-C and FR-4 layer in the MA structure.

As shown in Figure 6, the strongest absorption peaks are located at 9.4 and 12.5 GHz. Therefore, the distributions of the electric and magnetic fields at these frequencies are presented in Figures 7 and 8 to clarify the nature of absorption. Figure 7a,b show that of the magnetic field in the (**E**, **H**) and (**H**, **k**) planes, respectively, at the lower absorption frequency of 9.4 GHz. The corresponding one for the electric field in the (**E**, **k**) plane is in Figure 7c. It can be observed that the magnetic field is strongly excited at the corners of the MA structure. Specifically, the magnetic dipoles are seen along the direction of the incident **H**-field with electric half vortices at the same positions. The observed phenomena suggest that the absorption mode at 9.4 GHz is due to a magnetic-dipole Mie-resonance, caused by the dielectric resonator [22–27]. Figure 8 presents the distributions of the electric and magnetic fields in different planes at 12.5 GHz. The MA also exhibits the magnetic-dipole Mie-resonance, as indicated by the strong magnetic dipoles along the **H**-direction and the electric half vortices in the (**E**, **k**) plane. However, the locations of the magnetic dipoles at 12.5 GHz differ from those at 9.4 GHz. As shown in Figure 8, the induced magnetic dipoles are distributed in both center and outer edges of the MA structure, which are, of course, parallel to the **H**-direction.

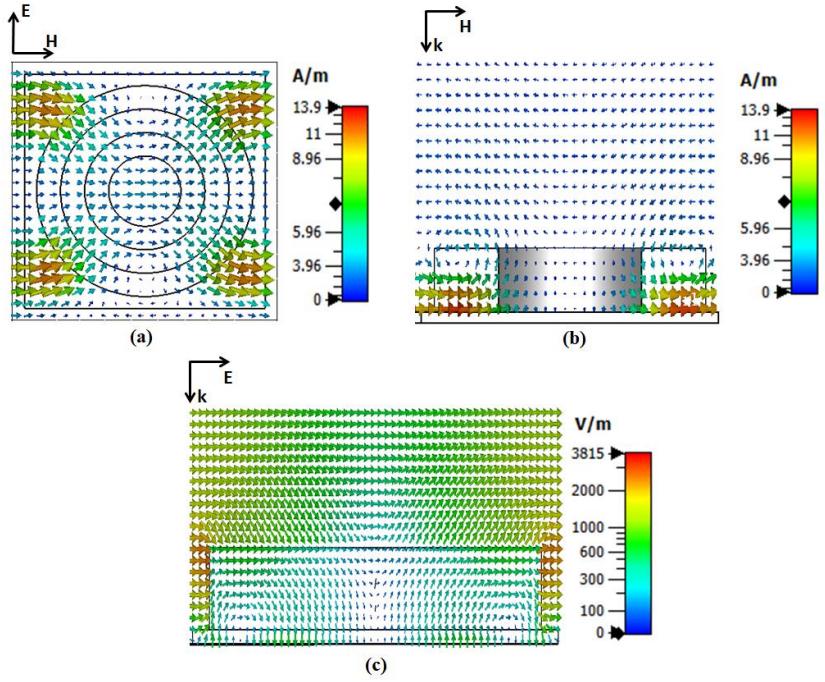

Figure 7. Electric- and magnetic-field distribution of the MA structure. (**a**) Magnetic field in the (**E**, **H**) plane, (**b**) magnetic field in the (**H**, **k**) plane, and (**c**) electric field in the (**E**, **k**) plane at a frequency of 9.4 GHz.

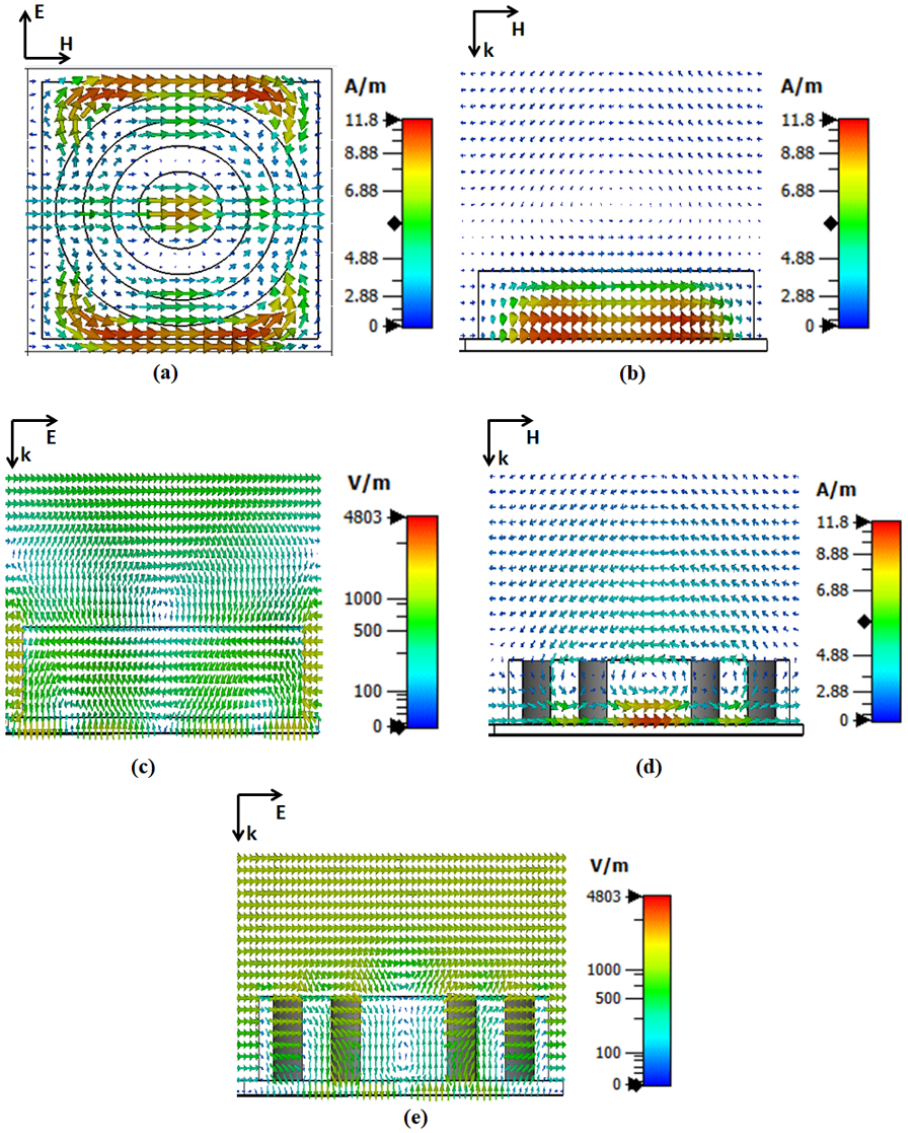

Figure 8. Electric and magnetic field distributions of the MA structure at a frequency of 12.5 GHz. (**a**) Magnetic field in the (**E**, **H**) plane. (**b**,**d**) Magnetic field in the (**H**, **k**) plane. (**c**,**e**) Electric field in the (**E**, **k**) plane.

To investigate the role of the real and imaginary parts of the complex permittivity (ε' and ε'') in the absorption mechanism, we analyzed the absorption characteristics of the MA structure by reducing the ε' and ε'' value to be 1/2, 1/4, and 1/6 of the original value, as illustrated in Figure 9. Initially, for the original ε' and ε'' values in Figure 2, the absorption spectrum showed a wide bandwidth of 7.9–14.6 GHz with an absorption exceeding 90%. As the ε' value is decreased, the absorption of the structure also decreases and the absorption peak shifts to a higher-frequency region [Figure 9a]. In addition, the reduction in the ε'' value results in the change in the absorption spectrum to be from the wideband to multi-band absorption [Figure 9b]. These results suggest that the real part of the FeCo-C permittivity mainly defines the frequency range of the absorption spectrum, while the imaginary part is responsible for the bandwidth of the absorption.

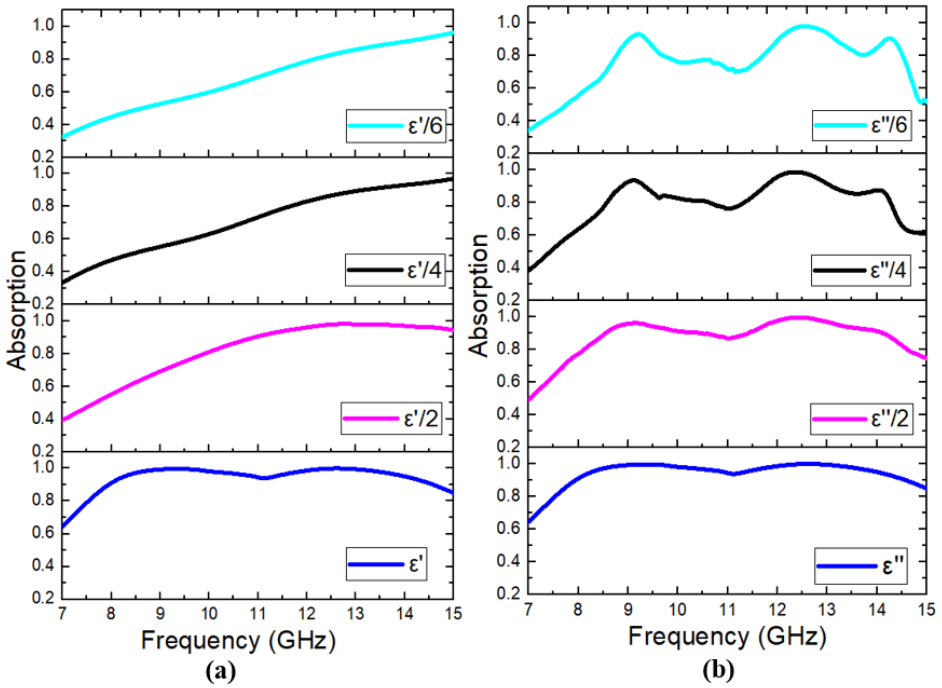

Figure 9. Absorption spectra of the MA corresponding to the (**a**) real and (**b**) imaginary parts of FeCo-C permittivity.

We also investigated the role of the real and imaginary parts of the complex permeability (μ' and μ'') on the absorption mechanism. The absorption characteristics of the MA structure according to the values of μ' and μ'' were simulated, as shown in Figure 10. Similarly, to the reduction in the real part of the permittivity, lowering the μ' value causes a shift in the absorption spectrum toward a higher-frequency range. However, the results in Figure 10b indicate that reducing the imaginary-part μ'' value does not significantly change the absorption spectrum of the MA. The nearly unchanged absorption, according to the imaginary part μ'', is due to its small value. Therefore, it can be concluded that the loss in our proposed MA is dominated by the imaginary part ε'' of FeCo-C.

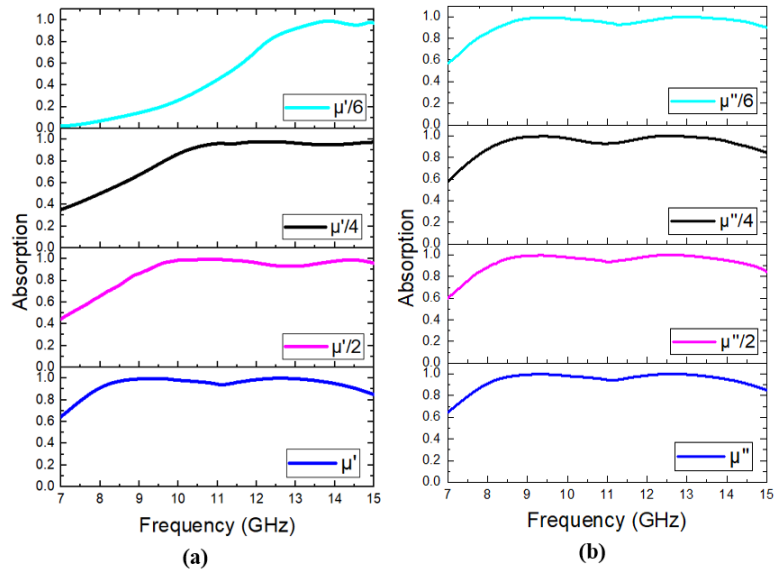

Figure 10. Absorption spectra of MA corresponding to the (**a**) real and (**b**) imaginary parts of FeCo-C permeability.

To evaluate the performance of the proposed MA structure, we also investigated the absorption spectra by varying the incident angle and polarization of the incoming EM wave. We found that the absorption spectrum was largely unaffected by the change in the polarization angle owing to the inherent symmetry of the structure, as shown in Figure 11a. However, the absorption of the MA is influenced by the incident angle, as indicated by a reduction in both the absorption magnitude and bandwidth [see Figure 11b,c]. Nonetheless, the proposed MA still reveals a good absorption property for both transverse-electric (TE) and transverse-magnetic (TM) polarization even at large incident angles. Specifically, for the TE polarization, the absorption decreases as the incidence angle increases from 0 to 55° but remains higher than 90% in a frequency range of from 8 to 11.1 GHz, as shown in Figure 11b. Similarly, in the TM mode, the absorption is maintained to be higher than 90% in a frequency region of from 9.5 to 14.6 GHz for incident angles up to 55°, as demonstrated in Figure 11c. As illustrated in Figure 11b,c, the absorption characteristics of the structure exhibit a more favorable behavior in the TM mode compared to the TE one. This observation can be rationalized by considering the orientation of the incident magnetic field. In the TM mode, the magnetic field direction remains fixed under the variation in the incident angle, while, in the TE one, the direction is no longer parallel to the sample plane and is deviated from it. The resonance mechanism of the MA structure is based on the magnetic-dipole Mie-resonance, indicating that the magnetic resonance of the MA structure is weakened as the angle of incidence increases. Consequently, sustaining the absorption in the TE mode is not as effective as it is in the TM one. These results reveal the high performance of the proposed MA, which is insensitive to the polarization of the incoming EM wave and is highly stable under the oblique incidence.

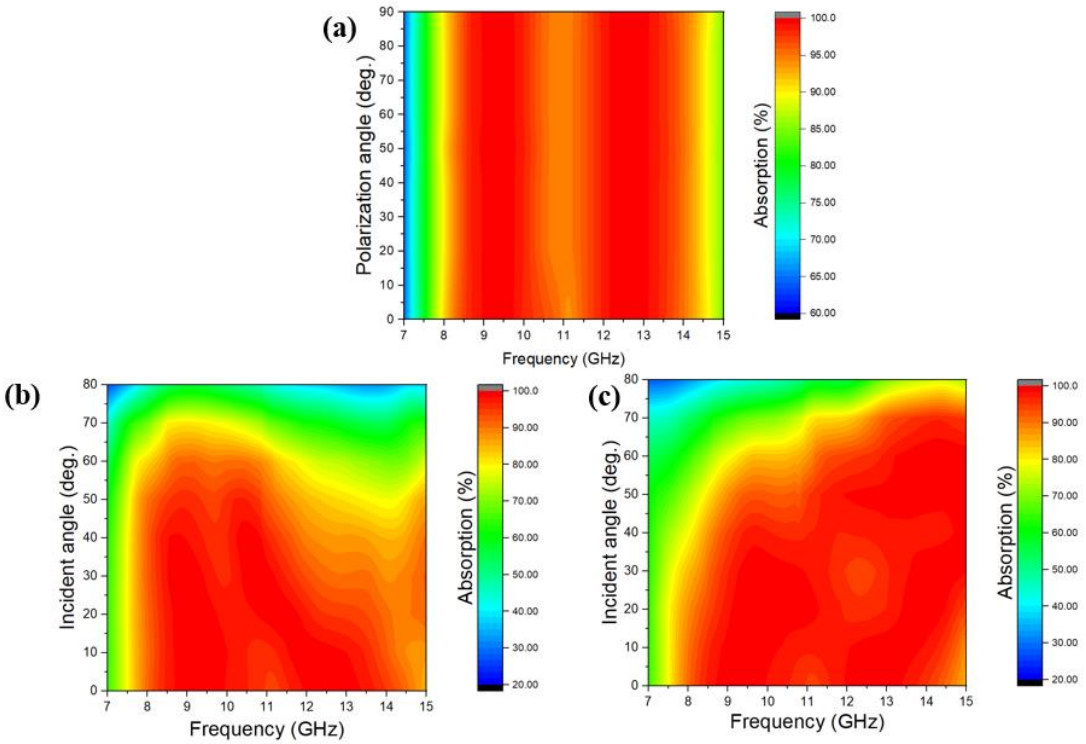

Figure 11. Dependence of the absorption spectrum of proposed MA on the (**a**) polarization angle at the normal incidence, and incident angle in the (**b**) TE and (**c**) TM polarization.

Finally, the absorption properties of the proposed MA are compared with those of the other absorbers reported previously (shown in Table 1), such as plain FeCo-C composites [20], FeCo/ZnO ones [28], Fe_3C/C nanofibers [29], and multi-walled carbon

nanotubes/nickel ferrite (MWCNTs/$NiFe_2O_4$) [30]. The efficient bandwidth (EBW) of the absorption is calculated as follows.

$$\text{EBW} = f_{high} - f_{low} \quad (1)$$

where f_{high} and f_{low} are the highest and lowest frequencies where the absorption is greater than 90%, respectively. The results indicate that our proposed absorber exhibits an enhanced absorption bandwidth, which can be attributed to not only the intrinsic properties of FeCo-C material but also the exploitation of the MA structure.

Table 1. Comparison of the microwave absorption bandwidth of proposed MA with those of other absorbers of different materials in previous studies.

Samples	EBW of Absorption (GHz)	Reference
FeCo/ZnO	5.1	[28]
Fe_3C/C	4.5	[29]
MWCNTs/$NiFe_2O_4$	3.8	[30]
plain FeCo-C	4.3	[20]
MA-based FeCo-C	6.7	This work

4. Conclusions

We demonstrated that the EM wave absorption properties of the FeCo-C alloy were enhanced by exploiting the metamaterial structure. The ultrabroadband absorption was achieved between 7.9 and 14.6 GHz, with an absorption above 90% in the case of the normal incidence of the incoming EM wave for all the polarization angles. The absorption remains to be above 90% in a frequency range of 8–11.1 GHz at wide angles of incidence from 0 to 55° for the TE polarization, while, in the TM mode, the absorption was also over 90% in a frequency range of 9.5–14.6 GHz. The physical mechanism of the proposed MA was elucidated, revealing that the high and ultrabroadband absorption was controlled by the magnetic-dipole Mie-resonances in the MA structure and the intrinsic EM properties of the FeCo-C material. Our work might contribute to the exploitation of various materials for the development of future MAs, which are used potentially for microwave applications in radar and telecommunication technology, as well as for EM shielding for health safety. Our work not only presents a comprehensive investigation of the obtained results in the scope of electromagnetics but might also hold potential significance in the broader context of broadband elastic/acoustic wave absorption. This is due to the correspondence between the constitutive parameters of the medium for propagating EM waves, namely, permittivity (ε) and permeability (μ), with mass density (ρ) and bulk modulus (κ), respectively [31,32]. Therefore, our findings might offer valuable insights and serve as a potential approach toward developing efficient broadband elastic/acoustic wave absorbers.

Author Contributions: T.X.D., B.S.T., B.X.K., V.D.L. and Y.L. conceived the idea. The electromagnetic simulation and calculation were carried out by T.X.D., B.S.T., B.X.K., N.T.N.A., H.Z., D.K.T., B.S.T., B.X.K., L.C., Y.L. and V.D.L. analyzed and wrote the article. All the authors discussed and commented on the manuscript. All authors have read and agreed to the published version of the manuscript.

Funding: This research is funded by Vietnam Academy of Science and Technology, under grant number VAST03.01/22-23, and by the Korea Evaluation Institute of Industrial Technology (Project No. 20016179).

Institutional Review Board Statement: Not applicable.

Informed Consent Statement: Not applicable.

Data Availability Statement: The data presented in this paper are available on request from the corresponding author.

Conflicts of Interest: The authors declare no conflict of interest. The funders had no role in the design of the study; in the collection, analyses, or interpretation of data; in the writing of the manuscript; or in the decision to publish the results.

References

1. Abdulkarim, Y.I.; Mohanty, A.; Acharya, O.P.; Bhargav, A.; Khan, M.S.; Mohapatra, S.K.; Muhammadsharif, F.F.; Dong, J. A Review on Metamaterial Absorbers: Microwave to Optical. *Front. Phys.* **2022**, *10*, 893791. [CrossRef]
2. Bregar, V.B.; Znidarsic, A.; Lisjak, D.; Drofenik, M. Development and Characterisation of an Electromagnetic Absorber. *Mater. Technol.* **2005**, *39*, 89–93.
3. Li, S.; Qiao, X.; Chen, J. Nano-Composite Electromagnetic Wave Absorbers. *J. Astr.* **2006**, *27*, 317–322.
4. Li, Y.; Liu, X.F.; Nie, X.Y.; Yang, W.W.; Wang, Y.D.; Yu, R.H. Multifunctional Organic–Inorganic Hybrid Aerogel for Self-Cleaning, Heat-Insulating, and Highly Efficient Microwave Absorbing Material. *Adv. Funct. Mater.* **2018**, *29*, 1807624. [CrossRef]
5. Landy, N.I.; Sajuyigbe, S.; Mock, J.J.; Smith, D.R.; Padilla, W.J. Perfect Metamaterial Absorber. *Phys. Rev. Lett.* **2008**, *100*, 207402. [CrossRef]
6. Hai, L.D.; Qui, V.D.; Tung, N.H.; Huynh, T.V.; Dung, N.D.; Binh, N.T.; Tuyen, L.D.; Lam, V.D. Conductive polymer for ultra-broadband, wide-angle, and polarization-insensitive metamaterial perfect absorber. *Opt. Expr.* **2018**, *26*, 33253. [CrossRef]
7. Akselrod, G.M.; Huang, J.; Thang, B.H.; Bowen, P.T.; Su, L.; Smith, D.R.; Mikkelsen, M.H. Large-Area Metasurface Perfect Absorbers from Visible to Near-Infrared. *Adv. Mater.* **2015**, *27*, 8028–8034. [CrossRef]
8. Park, J.H.; Park, C.; Lee, K.S.; Suh, S.J. Effect of NaOH and precursor concentration on size and magnetic properties of FeCo nanoparticles synthesized using the polyol method. *AIP Adv.* **2020**, *10*, 115220. [CrossRef]
9. Liu, X.G.; Geng, D.Y.; Meng, H.; Li, B.; Zhang, Q.; Kang, D.J.; Zhang, Z.D. Electromagnetic-wave-absorption properties of wire-like structures self-assembled by FeCo nanocapsules. *J. Phys. D Appl. Phys.* **2008**, *41*, 175001. [CrossRef]
10. Cheng, Y.; Ji, G.; Li, Z.; Lv, H.; Liu, W.; Zhao, Y.; Cao, J.; Du, Y. Facile synthesis of FeCo alloys with excellent microwave absorption in the whole Ku-band: Effect of Fe/Co atomic ratio. *J. Alloys Compd.* **2017**, *704*, 289–295. [CrossRef]
11. Wen, B.; Cao, M.S.; Hou, Z.L.; Song, W.L.; Zhang, L.; Lu, M.M. Temperature Dependent Microwave Attenuation Behavior for Carbon-Nanotube/Silica Composites. *Carbon* **2013**, *65*, 124–139. [CrossRef]
12. Kim, S.H.; Park, Y.G.; Kim, S.S. Double-Layered Microwave Absorbers Composed of Ferrite and Carbon Fiber Composite Laminates. *Phys. Stat. Sol. C* **2007**, *4*, 4602–4605. [CrossRef]
13. Chen, H.; Ma, W.; Huang, Z.; Zhang, Y.; Huang, Y.; Chen, Y. Graphene-Based Materials toward Microwave and Terahertz Absorbing Stealth Technologies. *Adv. Opt. Mat.* **2019**, *7*, 1801318. [CrossRef]
14. Huang, Z.; Chen, H.; Huang, Y.; Ge, Z.; Zhou, Y.; Yang, Y.; Xiao, P.; Liang, J.; Zhang, T.; Qian, S.; et al. Ultra-Broadband Wide-Angle Terahertz absorption properties of 3D graphene foam. *Adv. Funct. Mat.* **2018**, *28*, 1704363. [CrossRef]
15. Zhang, Y.; Huang, Y.; Chen, H.H.; Huang, Z.Y.; Yang, Y.; Xiao, P.S.; Zhou, Y.; Chen, Y.S. Composition and Structure Control of Ultralight Graphene Foam for High-Performance Microwave Absorption. *Carbon* **2016**, *105*, 438–447. [CrossRef]
16. Han, Z.; Li, D.; Wang, H.; Liu, X.G.; Li, J.; Geng, D.Y.; Zhang, Z.D. Broadband electromagnetic-wave absorption by FeCo/C nanocapsules. *Appl. Phys. Lett.* **2009**, *95*, 16–19. [CrossRef]
17. Han, Z.; Li, D.; Wang, X.W.; Zhang, Z.D. Microwave response of FeCo/carbon nanotubes composites. *J. Appl. Phys.* **2011**, *109*, 2009–2012. [CrossRef]
18. Jiang, J.J.; Li, X.J.; Han, Z.; Li, D.; Wang, Z.H.; Geng, D.Y.; Ma, S.; Liu, W.; Zhang, Z.D. Disorder-modulated microwave absorption properties of carbon-coated FeCo nanocapsules. *J. Appl. Phys.* **2014**, *115*, 2012–2015. [CrossRef]
19. Lv, H.; Ji, G.; Zhang, H.; Li, M.; Zuo, Z.; Zhao, Y.; Zhang, B.; Tang, D.; Du, Y. Co_xFe_y@C Composites with Tunable Atomic Ratios for Excellent Electromagnetic Absorption Properties. *Sci. Rep.* **2015**, *5*, 1–10. [CrossRef]
20. Su, X.G.; Wang, J.; Zhang, X.X.; Huo, S.Q.; Dai, W.; Zhang, B. Synergistic effect of polyhedral iron-cobalt alloys and graphite nanosheets with excellent microwave absorption performance. *J. Alloys Compd.* **2020**, *829*, 154426. [CrossRef]
21. Dassault Systemes. CST Studio Suite: Electromagnetic Field Simulation Software. Available online: http://www.cst.com (accessed on 15 June 2021).
22. Bohren, C.F.; Huffman, D.R. *Absorption and Scattering of Light by Small Particles*; John Wiley & Sons: New York, NY, USA, 2008.
23. Wang, Q.; Zhang, F.; Xiong, Y.J.; Wang, Y.; Tang, X.Z.; Jiang, C.; Abrahams, I.; Huang, X.Z. Dual-band binary metamaterial absorber based on low-permittivity all-dielectric resonance surface. *J. Electron. Mat.* **2019**, *48*, 787–793. [CrossRef]
24. Zhang, F.; Jiang, C.; Wang, Q.; Zhao, Z.; Wang, Y.; Du, Z.; Wang, C.; Huang, X. A multi-band closed-cell metamaterial absorber based on a low-permittivity all-dielectric structure. *Appl. Phys. Express* **2020**, *13*, 084001. [CrossRef]
25. Guo, M.C.; Wang, X.K.; Zhuang, H.Y.; Tang, D.M.; Zhang, B.S.; Yang, Y. 3D printed low-permittivity all-dielectric metamaterial for dual-band microwave absorption based on surface lattice resonances. *Phys. Scrip.* **2022**, *97*, 075504. [CrossRef]
26. Zhu, Y.Q.; Tian, X.; Fang, J.K.; Shi, Y.P.; Shi, S.N.; Zhang, S.; Song, J.M.; Li, M.P.; Liu, X.Y.; Wang, X.D.; et al. Independently tunable all-dielectric synthetic multi-spectral metamaterials based on Mie resonance. *RSC Adv.* **2022**, *12*, 20765–20770. [CrossRef]
27. Zhao, Q.; Kang, L.; Du, B.; Zhao, H.; Xie, Q.; Huang, X.; Li, B.; Zhou, J.; Li, L. Experimental Demonstration of Isotropic Negative Permeability in a Three-Dimensional Dielectric Composite. *Phys. Rev. Lett.* **2008**, *101*, 027402. [CrossRef]
28. Bao, X.; Wang, X.; Zhou, X.; Shi, G.; Xu, G.; Yu, J.; Guan, Y.; Zhang, Y.; Li, D.; Choi, C. Excellent microwave absorption of FeCo/ZnO composites with defects in ZnO for regulating the impedance matching. *J. Alloys Compd.* **2018**, *769*, 512–520. [CrossRef]

29. Jiang, Y.; Fu, X.; Zhang, Z.; Du, W.; Xie, P.; Cheng, C.; Fan, R. Enhanced microwave absorption properties of Fe_3C/C nanofibers prepared by electrospinning. *J. Alloys Compd.* **2019**, *804*, 305–313. [CrossRef]
30. Zhang, J.; Shu, R.; Guo, C.; Sun, R.; Chen, Y.; Yuan, J. Fabrication of nickel ferrite microspheres decorated multi-walled carbon nanotubes hybrid composites with enhanced electromagnetic wave absorption properties. *J. Alloys Compd.* **2019**, *784*, 422–430. [CrossRef]
31. Ma, G.; Sheng, P. Acoustic metamaterials: From local resonances to broad horizons. *Sci. Adv.* **2016**, *2*, e1501595. [CrossRef]
32. Wang, X.; Guo, Y.; Bousba, S. Direct imaging for the moment tensor point sources of elastic waves. *J. Comput. Phys.* **2022**, *448*, 110731. [CrossRef]